THE JOURNAL OF PHYSICAL CHEMISTRY LETTERS
A JOURNAL OF THE AMERICAN CHEMICAL SOCIETY

pubs.acs.org/JPCL

Letter

Structure and Dynamics of RNA Guanine Quadruplexes in SARS-CoV-2 Genome. Original Strategies against Emerging Viruses

Tom Miclot, Cécilia Hognon, Emmanuelle Bignon, Alessio Terenzi, Marco Marazzi, Giampaolo Barone,* and Antonio Monari*

Cite This: *J. Phys. Chem. Lett.* 2021, 12, 10277−10283

Read Online

ACCESS | Metrics & More | Article Recommendations | Supporting Information

ABSTRACT: Guanine quadruplex (G4) structures in the viral genome have a key role in modulating viruses' biological activity. While several DNA G4 structures have been experimentally resolved, RNA G4s are definitely less explored. We report the first calculated G4 structure of the RG-1 RNA sequence of SARS-CoV-2 genome, obtained by using a multiscale approach combining quantum and classical molecular modeling and corroborated by the excellent agreement between the corresponding calculated and experimental circular dichroism spectra. We prove the stability of the RG-1 G4 arrangement as well as its interaction with G4 ligands potentially inhibiting viral protein translation.

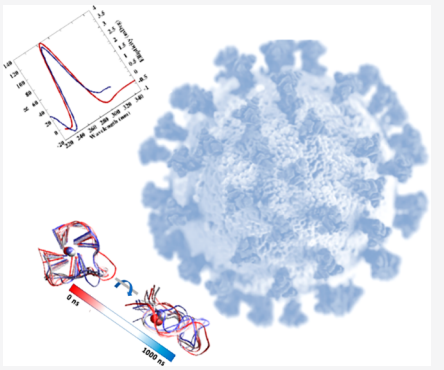

At the end of 2019, a sudden outbreak of Severe Acute Respiratory Syndrome (SARS) developed in mainland China[1] and further spread worldwide, obliging the World Health Organization (WHO) to declare the emergence of a pandemic in March 2020. The syndrome is caused by a novel coronavirus, SARS-CoV-2, and has been styled COVID-19.[2,3] Despite the relatively low mortality, SARS-CoV-2 is highly contagious, and COVID-19 can evolve into severe forms necessitating critical care. Hence, COVID-19 is causing a considerable strain on healthcare systems, requiring unprecedented large-scale social distancing and containment measures, including full lock-downs. Even though vaccines have been promptly developed and released,[4] including the emergent mRNA (mRNA) technology,[5] COVID-19 is still raging worldwide as of summer 2021, pushed by the emergence of more contagious viral strains, such as the Δ variant, which has become notably dominant in Europe and the United States. The harmful effects of COVID-19 are also aggravated by the fact that no clearly efficient and safe antiviral agent has been proposed for large-scale use. Indeed, while some nucleoside analogues, including Remdesivir, have shown high antiviral efficiency *in vitro* and *in vivo*, related side-effects strongly hamper their diffusion.[6] In parallel to the mobilization of the medicinal chemistry community,[7] several structural biology[8] as well as molecular modeling and simulation[9] groups have produced an unprecedented effort, which has allowed the resolution and characterization of the main SARS-CoV-2 structural and nonstructural proteins.

The rather complex organization of the viral genome, also in the case of RNA viruses, has been recently highlighted and related to their biological functions. In particular, the presence of guanine-quadruplexes (G4) arrangements has been spotlighted.[10]

G4 arrangements are common in guanine-rich regions and are achieved by a superposition of planes composed of four guanines (tetrads) which are stabilized by the formation of Hoogsten-type hydrogen bond and by the interaction with cations placed in the central canal.[11,12] G4s have been recently associated with important roles,[13−15] such as the protection of telomeric regions in DNA[16] and the control of gene expression, and have also been highlighted in viruses.[17] The presence of quadruplexes' folding may preserve the viral genetic material, avoiding its recognition by the immune system. On the other hand, it has been shown that an overstabilization of G4s may inhibit the translation of viral proteins by the cellular apparatus. In the case of SARS-type coronaviruses, it has also been shown that the highly conserved SARS unique domain (SUD), used to sequestrate pro-apoptotic cellular mRNA sequences, is maintained in its active dimeric form by the interaction with G4 RNA sequences.[18−20] In fact, while SARS-CoV-2 genome is to some extent less prone to arrange in quadruplexes, compared to other viruses such as Zika,[21] four putative G4 sequences have been recently

Received: September 17, 2021
Accepted: October 14, 2021

https://doi.org/10.1021/acs.jpclett.1c03071
J. Phys. Chem. Lett. 2021, 12, 10277−10283

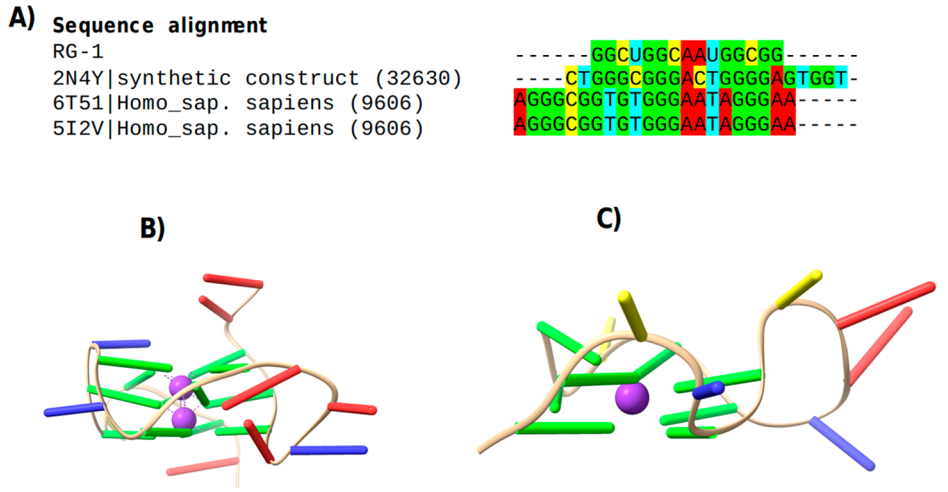

Figure 1. (A) Alignment of RG-1 sequence with a synthetic construct from HIV-1 genome (2N4Y) and two *Homo sapiens* DNA G4s sequences (6T51 and 5I2 V). (B) Side view of the structure of the G4 DNA from PDB 6T51 and (C) of the reconstructed RG-1. The stabilizing K^+ ions, which are included in the simulation, are represented in purple.

evidenced by Zhao et al.[22] In particular the so-called RG-1 sequence, located in the nucleocapsid (N) protein coding region, has been characterized using electronic circular dichroism (ECD). The presence of G4s in infected living cells has also been confirmed, and their stabilization by ligands can induce the downregulation of their expression, impairing the maturation and infectivity of viral proteins, hence paving the way to appealing therapeutic strategies.

Despite the importance of RNA G4 in the biological cycle of viruses like SARS-CoV-2, their structural characterization usually remains elusive. This is also underlined by the relative scarce number of RNA G4 structures that have been resolved, especially compared to their DNA counterparts. At the same time, the high ECD sensitivity to secondary structure rearrangements allows achieving a molecular resolution giving access to all the subtle structural factors that may be crucial in driving the possible interactions with external ligands. In this Letter, we study the RG-1 sequence through a combination of multiple sequence alignment, homology modeling, classical molecular dynamics (MD), and hybrid quantum mechanics/molecular mechanics (QM/MM), in order to disentangle all the structural factors associated with the G4 conformations, and by comparing the time-dependent density functional theory (TD-DFT) simulated ECD spectrum with the experimental one by Zhao et al.[23] The full computational strategy of our multiscale approach can be found in the Supporting Information.

The structure of RG-1 was predicted from a multiple sequence alignment with three DNA G4 sequences corresponding to experimental structures (PDB codes 2N4Y,[24] 6T51,[25] 5I2V).[26] The RG-1 structural model exhibits a parallel G4 composed of two superposed tetrads (see Figure 1). Interestingly, we can also evidence that, in addition to the G4 core, a rather large nonstructured loop, composed of adenines and cytosines, is also present as a linker to the guanines involved in the tetrad. The same loop is also present on the human DNA G4 used as template (PDB 6T51) (see Figure 1B). Three independent 1 μs MD trajectories of the RG-1 G4 model solvated in a periodic box of TIP3P water[27] have been run using the amber f99 force field including the parmbsc0[28] and the χOL3[29] corrections to take into account the specific RNA features. In addition simulations performed modeling the nucleic acid with the bsc1 corrections,[28,30] i.e., with force field specifically designed for DNA, have also been performed. All the simulations have been carried out with the NAMD code.[31] For sake of clarity, the results of all the replicas are collected in Table 1, in the form of average and standard deviation of the most crucial structural parameters. The time series of the same parameters are also presented in Figure 2 for the first replica while the other two, which exhibit identical trends, can be found in the Supporting Information.

From our MD simulations, the RG-1 tetrad core is extremely stable and experiences only slight vibrational deformation (see

Table 1. Average and Standard Deviation of the Main Structural Parameters for the RG-1 Simulations in the Three Replicas[a]

	replica 1	replica 2	replica 3
RMSD nucleic (Å)	4.66 ± 1.00	5.46 ± 1.07	5.79 ± 1.07
RMSD tetrads (Å)	1.63 ± 0.33	1.71 ± 0.24	1.81 ± 0.33
tetrad distance (Å)	3.43 ± 0.086	3.46 ± 0.08	3.46 ± 0.10
Ω (deg)	31.16 ± 2.42	31.30 ± 2.53	31.13 ± 2.44
	α Tetrad		
$\theta_{G1\text{-}G15}$ (deg)	89.95 ± 4.29	92.70 ± 4.89	91.36 ± 4.43
$\theta_{G11\text{-}G14}$ (deg)	88.96 ± 4.32	89.03 ± 4.80	90.64 ± 5.17
$\theta_{G5\text{-}G11}$ (deg)	89.14 ± 4.44	89.45 ± 4.49	89.07 ± 4.39
$\theta_{G5\text{-}G14}$ (deg)	92.80 ± 4.09	89.88 ± 4.24	90.21 ± 4.62
$\theta'_{G1\text{-}G14}$ (deg)	170.15 ± 5.81	170.26 ± 5.71	169.73 ± 6.76
$\theta'_{G1\text{-}G11}$ (deg)	167.97 ± 6.82	165.98 ± 7.76	165.88 ± 8.59
	β Tetrad		
$\theta_{G2\text{-}G6}$ (deg)	88.50 ± 3.98	90.94 ± 4.67	89.48 ± 4.24
$\theta_{G12\text{-}G15}$ (deg)	89.18 ± 4.61	90.39 ± 4.65	89.52 ± 4.49
$\theta_{G6\text{-}G12}$ (deg)	90.44 ± 4.21	91.19 ± 4.48	90.33 ± 4.10
$\theta_{G6\text{-}G15}$ (deg)	94.31 ± 4.51	92.29 ± 4.46	93.71 ± 7.89
$\theta'_{G2\text{-}G15}$ (deg)	165.90 ± 9.61	163.52 ± 9.97	163.89 ± 12.94
$\theta'_{G2\text{-}G12}$ (deg)	163.14 ± 9.62	159.83 ± 10.22	164.21 ± 9.42

[a]The values of the θ and θ' angles are reported for each of the couple of guanines constituting the tetrads. The distance between the tetrads is considered as the distance between the center of mass of each quartet.

https://doi.org/10.1021/acs.jpclett.1c03071
J. Phys. Chem. Lett. 2021, 12, 10277−10283

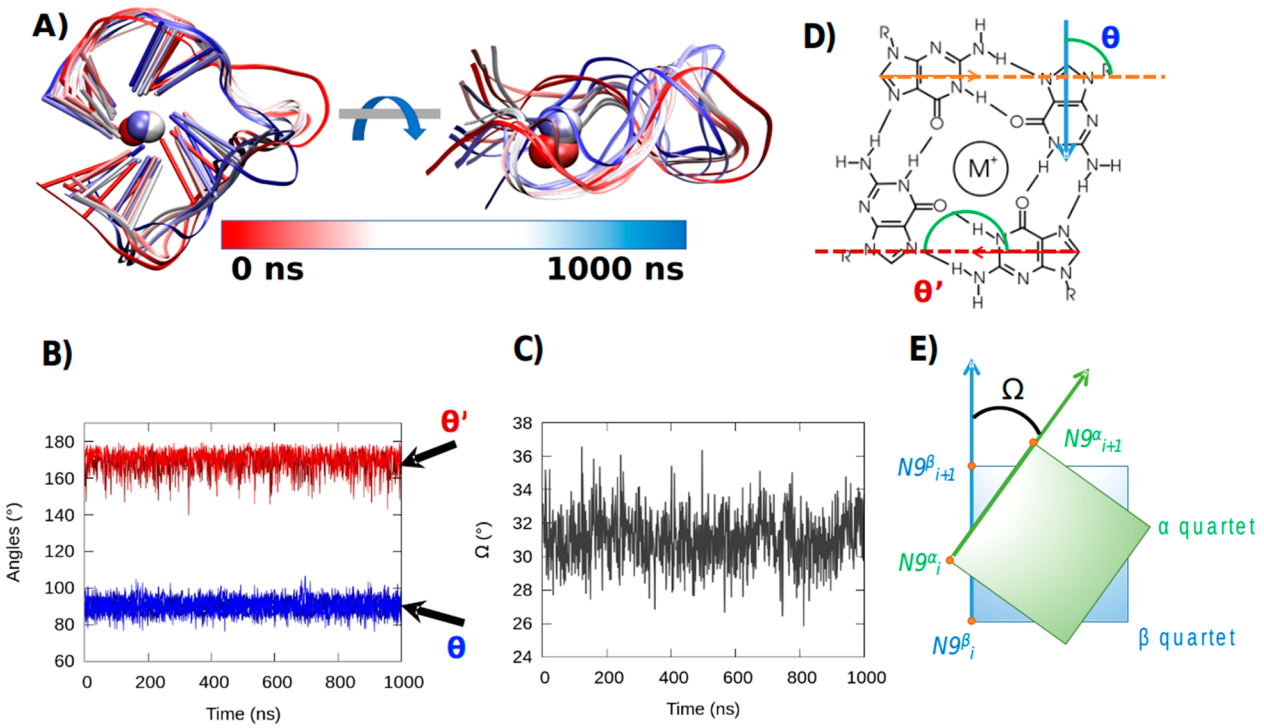

Figure 2. (A) Representative snapshots of the RG-1 RNA G4 extracted along the MD trajectory for the first replica. The color code represents the time evolution. Time evolution of the θ and θ' angles for the first, α, tetrad (B) and of the twist angle Ω (C). Schematic depiction of θ and θ' angles indicating the arrangement of guanines on the tetrad (D) and of the twist angle Ω (E). The results for the other replica and for the bsc1 force field are found in the Supporting Information and in Table 1.

Figure 2A). As expected, the connecting loop is much more flexible and accesses a larger conformational space. Interestingly, the fluctuations of this loop also lead to some metastable states in which adenines and cytosines can be π-stacked to the guanines in the tetrad.

Core rigidity and loop flexibility can also be inferred from the analysis of the root mean square deviation (RMSD) which is larger for the whole nucleic acid system than for the tetrad only. While the RG-1 sequence presents a moderate RMSD peak at around 8.0 Å, this value is mainly due to the contribution of the peripheral loop, which amounts to 5.8 Å. In contrast, the RMSD of the nucleobases in the tetrads barely reaches 1.8 Å, highlighting the negligible deviation of the tetrad core from the original starting conformation. As usual in G4 arrangements, the rigidity of the central core is due to the involvement of the guanines in the Hoogsteen hydrogen bonding network and to the favorable interaction with the metal cations present in the central channel. Of note, the same rigidity of the central core, combined with the flexibility of the peripheral loops, can also be observed from the 2-dimensional (2D) RMSD map reported in the Supporting Information.

The stability of G4 arrangement is reflected in the almost ideal values assumed by the θ and θ' angles defining the disposition of the guanines in the tetrad (see Figure 2D and Table 1). θ peaks at around 90°, and θ' is centered around 160° in both tetrads (see Figure 2-B, Table 1, and the Supporting Information). Furthermore, the standard deviations are relatively small, not exceeding 5°, and the values are coherently reproduced for all the replicas (Table 1). Such a situation is indicative of the formation of a stable and persistent Hoogsteen hydrogen bonding network, hence confirming the propensity of the RG-1 RNA sequence to assume a G4 parallel conformation. As a more global descriptor, the stability and rigidity of the G4 core is also reflected by the time evolution of the Ω angle describing the twisting between the two tetrads (Figure 2C,E), which is centered around the ideal value of 31° typical of a parallel arrangement, while the standard deviation is close to 2°. Importantly, once again the distribution of the parameter is coherently reproduced in all the replicas (Table 1 and the Supporting Information).

Behaviors similar to the ones reported in Figure 2 and Table 1 are observed when using the DNA-based bsc1 force field (see the Supporting Information), providing further proof of the robustness of our approach. Furthermore, by performing clustering of the trajectories of the independent replicas, we also confirm that the conformational space explored by our system is strongly overlapping.

Hence, our MD trajectories are coherent with the experimental data in confirming the possible folding of the RG-1 sequence of the SARS-CoV-2 genome into a parallel G4 conformation. In their original work, Zhao et al.[23] used ECD spectroscopic signatures to confirm the structuration of the RNA sequence into a G4 arrangement. To allow a better mapping between molecular modeling and experimental results we have simulated the ECD spectrum using a hybrid QM/MM approach on top of snapshots extracted from the MD trajectory. The simulation of ECD spectra from snapshots obtained from a classical sampling of the chromophore phase-space has been successfully used by our group for related systems;[32−34] however, in the previous contribution the rotatory strength and the excitation energies of the multi-chromophoric aggregates have been obtained considering an excitonic coupling Hamiltonian. Although powerful, the excitonic model is inherently semiempirical, especially in its dipole approximation, hence leading to a suboptimal

https://doi.org/10.1021/acs.jpclett.1c03071
J. Phys. Chem. Lett. 2021, 12, 10277−10283

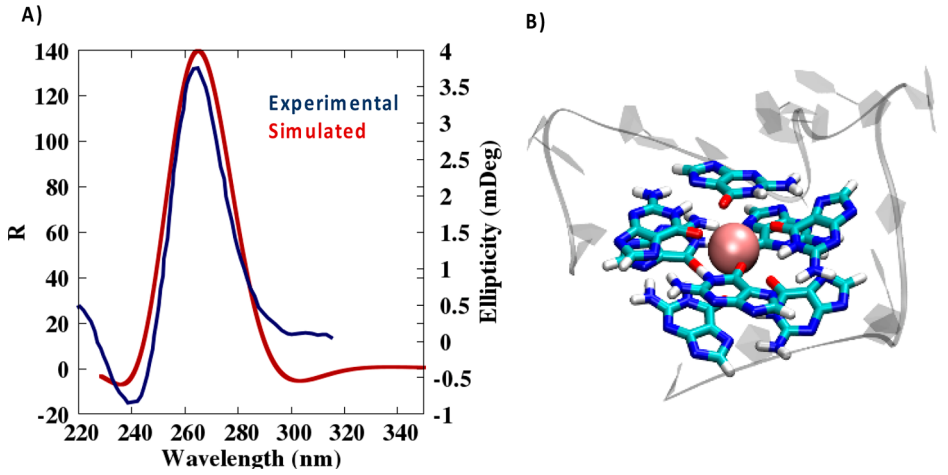

Figure 3. (A) Experimental, from Zhao et al.,[23] and simulated ECD spectrum of the RG-1 RNA sequence. Note that the simulated spectrum has been homogeneously shifted by 40 nm. The simulated spectrum is obtained by QM/MM at the TD-DFT level with M06-2X functional and the 6-31G(d) basis, calculating 60 excited states. (B) The chosen QM partition is highlighted in ball and stick representation, while the G4 backbone and dangling bases are shown in cartoon from.

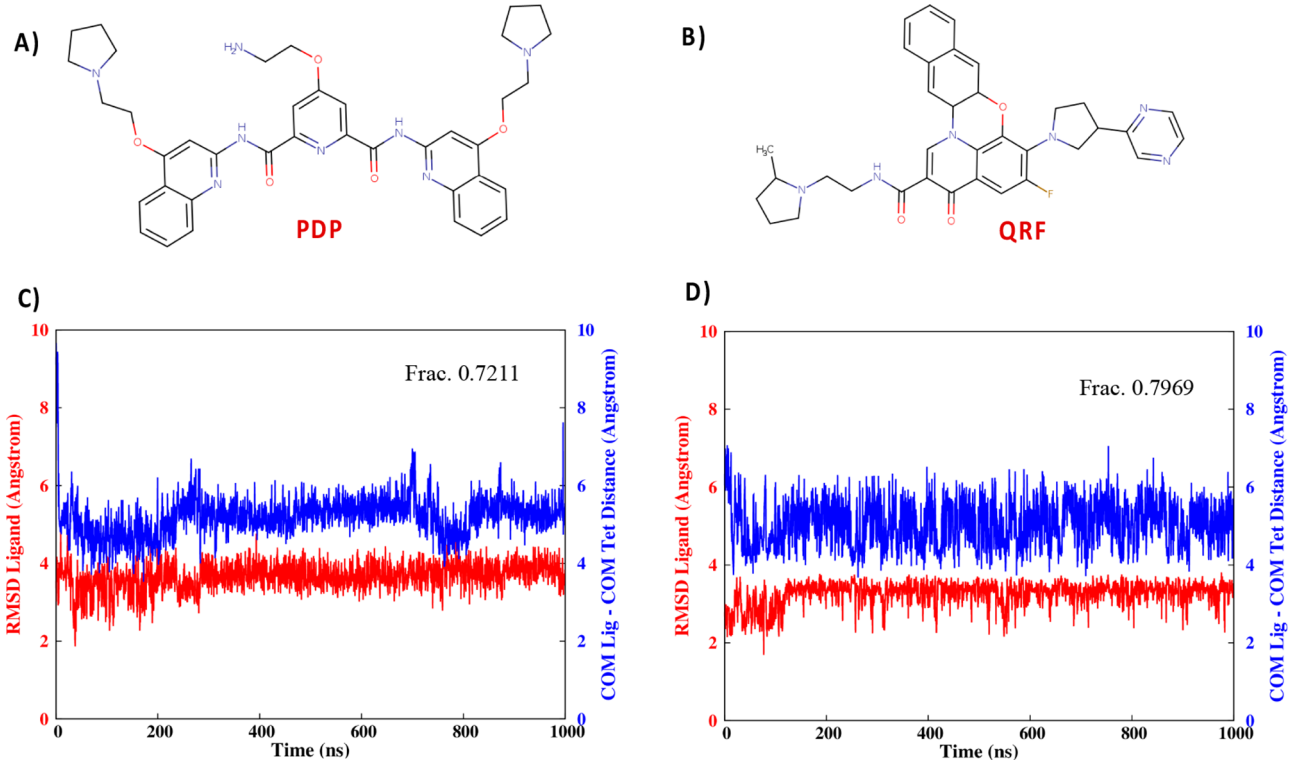

Figure 4. Chemical representation of quarfloxin, QRF (A), and pyridostatin, PDP (B), together with the most important conformation obtained from clustering of the ligand bound to G4, the time evolution of the RMSD, and the time evolution of the distance between the center of mass of the ligands and of the tetrads (C and D for QRF and PDP, respectively). Note that the RMSD is calculated from the starting frame.

description of relatively strongly coupled multichromophores. Furthermore, some dependency on the partitioning of the system can still be observed in the final results. For these reasons, we decide to bypass this problem by using a fully *ab initio* approach and including all the stacked nucleobases in the QM partition. The QM/MM excited-state calculations have been performed using the Orca/Amber interface, and the eight nucleobases forming the G4 core have been included in the QM partition to consider the coupling between the π-stacked chromophores (Figure 3B). Although we have applied a shift to the calculated absorption wavelengths, the results, in terms of band shape, are in good agreement with the experimental spectrum published by Zhao et al.[23] (see Figure 3). The experimental spectrum presents a first large and rather intense positive peak centered around 270 nm followed by a negative peak at 240 nm, whose intensity is much smaller, the ratio being about 1:4. Such a pattern is common in the case of nucleic acid aggregates and can be seen as a typical spectroscopic feature of parallel G4 arrangement. The results of our QM/MM simulation produced an ECD spectrum with a similar pattern, but with blue-shifted signals, due to the use of a reduced basis set.

https://doi.org/10.1021/acs.jpclett.1c03071
J. Phys. Chem. Lett. 2021, 12, 10277−10283

Although a larger basis set could reproduce with more precision the absorption energy, in the context of the present work we considered of more prominence the correct description of the global shape of the ECD signal, thus confirming the G4 conformation, at the same time correctly describing the electronic nature of the spectral signature.

The choice of the basis set was imposed not only by the computational overload due to the extended QM partition but also by the necessity to avoid QM wave function over-polarization due to the interaction with the MM point charges. To palliate the basis set incompleteness, we apply a global shift of 45 nm to the simulated ECD signal to allow the straightforward comparison with the experimental counterpart (see Figure 3). As for the choice of the exchange−correlation functional in Figure S4 we report the simulated ECD spectra, obtained on top of the *bsc*1-based trajectory with hybrid, long-range corrected, and meta-hybrid functionals, illustrating the superiority of M06-2X over the other choices. The similarities between the simulated and experimental signals in Figure 3 are self-evident, providing a clear picture in terms of the relative position of the two main peaks, their intensity, and the global band shape: a broad positive band is followed by a less intense, and slightly sharper, negative signal. However, the higher-energy negative band has a reduced intensity probably due to the necessity of calculating a larger number of excited states. The globally good agreement between the calculated and experimental spectra, despite the applied energy shift, supports the folding of the RG-1 sequence in a parallel G4 conformation.

Having shown the stability and the persistence of the G4 arrangements, the question arises whether some ligands could interact with the RG-1 RNA sequence and possibly over-stabilize it to induce an effective inhibition of the translation of the viral genome and impair the viral cycle. In this context, we have examined the interaction of two ligands with the RG-1 sequence, namely, quarfloxin (QRF) and pyridostatin (PDP). QRF (also called CX-3543) is a well-known G4-binding ligand, believed to target RNA G4s and evaluated in phase II clinical trials for human cancer therapy.[35] PDP is also known for its capacity to modulate the expression of G4 containing genes, providing antiproliferative effects.[36] Interestingly, PDP was reported by Zhao et al.[23] as a ligand capable of selectively recognizing RG-1 and increase its melting temperature. The initial complexes between RG-1 and the two ligands have been obtained by docking the drugs onto the parallel G4 structure. The stability of each significant pose has been further confirmed running two independent 1 μs MD trajectories. Representative structures of the main binding modes are reported in Figure 4, and the results for a slightly different initial pose, in which the ligand interacts with the tetrad, are also collected in the Supporting Information.

Both the docking and the MD simulations agree in previewing the formation of stable complexes between the RNA G4 and the small ligands, the persistence and stability of which can also be appreciated by the extended plateau observed on the RMSD time-series after 400 ns (Figure 4B,D). More importantly, it can be observed that the binding takes place via π-stacking of the ligand on top of the tetrad plans, and it is mostly driven by dispersion and hydrophobic interactions. This result can be rationalized by the presence of conjugated moieties on the ligands and their globally planar structure. Furthermore, such interaction modes, while providing an enhanced stabilization of the G4 arrangement due to the increase of the attractive interactions, induce only moderate or negligible structural perturbation as can also be observed from the angles between the guanines and the twist reported in the Supporting Information for the different interaction modes and ligands. The structural stability of the G4 arrangement upon binding with ligands is also consistent with the experimental results that showed only slight differences in the ECD spectra upon interaction of RG-1 with PDP. In addition, the π-stacking interaction, also due to the largely aromatic nature of both ligands, is susceptible to take place without any important energetic barrier, or steric hindrance, hence greatly facilitating the recruitment of the drug. While incontestably pointing toward the formation of stable complexes, the results of the equilibrium MD simulations alone cannot underlie any significant or qualitative difference between QRF and PDP binding, hence suggesting that both can potentially be seen as valuable ligands to stabilizing G4 arrangements and more particularly the parallel conformation of the RG-1 RNA sequence. The stability of the complex and the presence of a dominant structure can also be evidenced by the clustering and the 2DRMSD reported in the Supporting Information. Indeed, as shown in Figure 4B,D we may see that the distance between the center of mass of the ligand and of the G4 tetrad is remarkably stable all along the trajectory. Notably, the dominant conformation obtained by clustering and corresponding to a bound complex is also accounting for about 80% for both drug candidates. However, the dominant interactions exhibited by the two ligands are rather unspecific, mainly driven by π-stacking, and should be taken as a proof of concept of the possible stabilization of the G4 structure. From a medicinal and drug-design point of view, it seems reasonable to infer that common, and known, G4-ligands could potentially affect SARS-CoV-2 replication. Furthermore, the increase of the π-conjugation and the presence of the fused aromatic ring, as well as a planar structure, appears as the most important characteristics for a potentially interesting lead compound.

We have unravelled the structural behavior of a putative G4 RNA sequence present in the genome of SARS-CoV-2 using multiscale molecular modeling approaches. The combination of the multiple sequence alignment, the microsecond-scale sampling of the conformational space, and computational spectroscopy support the fact that the RG-1 sequence may adopt a stable parallel G4 conformation composed of two rigid tetrads and a flexible peripheral loop. Our results point to the fact that the rigid core is reliably sampled, in the limits of the force field accuracy. The more flexible loop may experience also further conformations and is essentially disordered. However, this effect cannot be captured by the ECD spectrum which is mostly due to the effect of the stacked guanine nucleobases. This is clearly even more stringent for the simulated spectrum in which the loop is not included in the QM partition. In addition, we have shown that the G4 conformation can, without any major structural rearrangement, form stable complexes with known G4 ligands, which are susceptible to increase the persistence of the quadruplex structure. The important role of G4s in tuning the viral response and the biological cycle, including emerging RNA viruses such as Zika, Dengue, or coronaviruses, calls for the precise determination of putative G4 sequences. Moreover, influencing the equilibrium between unfolded and G4 sequences via the use of small drugs offers an original, yet not fully explored, possibility for the development of novel and

https://doi.org/10.1021/acs.jpclett.1c03071
J. Phys. Chem. Lett. 2021, 12, 10277−10283

potentially wide-action antiviral agents. This study highlights the robustness of our *in silico* protocol to provide a most favorable complement to experimental studies in suggesting specific interaction modes and structures of RNA sequences. Our contribution represents a proof of concept of the capacities offered by mature and multiscale simulation techniques to unravel key biological processes and phenomena.

■ ASSOCIATED CONTENT

Supporting Information

The Supporting Information is available free of charge at https://pubs.acs.org/doi/10.1021/acs.jpclett.1c03071.

Protocol of the sequence and sequence-structure analysis, additional details of the MD and QM/MM simulations, RNA G4 structural parameters for the different replicas, different force fields, unshifted ECD spectra, 2D-RMSD, and clustering (PDF)

Pdb of RG-1 structure bound and unbound to the ligands (ZIP)

■ AUTHOR INFORMATION

Corresponding Authors

Giampaolo Barone − *Department of Biological, Chemical and Pharmaceutical Sciences, University of Palermo, 90126 Palermo, Italy;* orcid.org/0000-0001-8773-2359; Email: giampaolo.barone@unipa.it

Antonio Monari − *Université de Lorraine and CNRS, UMR 7019 LPCT, F-54000 Nancy, France; Université de Paris and CNRS, Itodys, F-75006 Paris, France;* orcid.org/0000-0001-9464-1463; Email: Antonio.monari@univ-lorraine.fr

Authors

Tom Miclot − *Department of Biological, Chemical and Pharmaceutical Sciences, University of Palermo, 90126 Palermo, Italy; Université de Lorraine and CNRS, UMR 7019 LPCT, F-54000 Nancy, France*

Cécilia Hognon − *Université de Lorraine and CNRS, UMR 7019 LPCT, F-54000 Nancy, France*

Emmanuelle Bignon − *Université de Lorraine and CNRS, UMR 7019 LPCT, F-54000 Nancy, France;* orcid.org/0000-0001-9475-5049

Alessio Terenzi − *Department of Biological, Chemical and Pharmaceutical Sciences, University of Palermo, 90126 Palermo, Italy;* orcid.org/0000-0001-9751-1373

Marco Marazzi − *Departamento de Química Analítica, Química Física e Ingeniería Química, Universidad de Alcalá, E-28805 Madrid, Spain; Instituto de Investigación Química "Andrés M. del Río" (IQAR), Universidad de Alcalá, E-28871 Madrid, Spain;* orcid.org/0000-0001-7158-7994

Complete contact information is available at: https://pubs.acs.org/10.1021/acs.jpclett.1c03071

Notes

The authors declare no competing financial interest.

■ ACKNOWLEDGMENTS

The work has been conducted via the financial support of the Universities of Palermo and Lorraine and the French CNRS. T.M. thanks the University of Palermo for granting a Ph.D. fellowships. Calculations have been partially performed on the local LPCT computing cluster and on the Regional Explor Computing Center. The authors thank GENCI for providing access to the national computing center under the project "Seek&Destroy". M.M. is grateful to the University of Alcalá for providing funds under the COVID-19 project 2020/00256/001. E.B. and A.M. thank the CNRAS and the French Research Ministry (MESRI) for funding under the GAVO project.

■ REFERENCES

(1) Zhu, N.; Zhang, D.; Wang, W.; Li, X.; Yang, B.; Song, J.; Zhao, X.; Huang, B.; Shi, W.; Lu, R.; et al. A Novel Coronavirus from Patients with Pneumonia in China, 2019. *N. Engl. J. Med.* **2020**, *382* (8), 727−733.

(2) Hu, B.; Guo, H.; Zhou, P.; Shi, Z. L. Characteristics of SARS-CoV-2 and COVID-19. *Nat. Rev. Microbiol.* **2021**, *19* (3), 141−154.

(3) Harapan, H.; Itoh, N.; Yufika, A.; Winardi, W.; Keam, S.; Te, H.; Megawati, D.; Hayati, Z.; Wagner, A. L.; Mudatsir, M. Coronavirus Disease 2019 (COVID-19): A Literature Review. *J. Infect. Public Health* **2020**, *13* (5), 667−673.

(4) Forni, G.; Mantovani, A.; Forni, G.; Mantovani, A.; Moretta, L.; Rappuoli, R.; Rezza, G.; Bagnasco, A.; Barsacchi, G.; Bussolati, G.; et al. COVID-19 Vaccines: Where We Stand and Challenges Ahead. *Cell Death Differ.* **2021**, *28* (2), 626−639.

(5) Topol, E. J. Messenger RNA Vaccines against SARS-CoV-2. *Cell* **2021**, *184* (6), 1401.

(6) Beigel, J. H.; Tomashek, K. M.; Dodd, L. E.; Mehta, A. K.; Zingman, B. S.; Kalil, A. C.; Hohmann, E.; Chu, H. Y.; Luetkemeyer, A.; Kline, S.; et al. Remdesivir for the Treatment of Covid-19 — Final Report. *N. Engl. J. Med.* **2020**, *383* (19), 1813−1826.

(7) Gil, C.; Ginex, T.; Maestro, I.; Nozal, V.; Barrado-Gil, L.; Cuesta-Geijo, M. Á.; Urquiza, J.; Ramírez, D.; Alonso, C.; Campillo, N. E.; et al. COVID-19: Drug Targets and Potential Treatments. *J. Med. Chem.* **2020**, *63* (21), 12359−12386.

(8) Arya, R.; Kumari, S.; Pandey, B.; Mistry, H.; Bihani, S. C.; Das, A.; Prashar, V.; Gupta, G. D.; Panicker, L.; Kumar, M. Structural Insights into SARS-CoV-2 Proteins. *J. Mol. Biol.* **2021**, *433* (2), 166725.

(9) Francés-Monerris, A.; Hognon, C.; Miclot, T.; García-Iriepa, C.; Iriepa, I.; Terenzi, A.; Grandemange, S.; Barone, G.; Marazzi, M.; Monari, A. Molecular Basis of SARS-CoV-2 Infection and Rational Design of Potential Antiviral Agents: Modeling and Simulation Approaches. *J. Proteome Res.* **2020**, *19* (11), 4291−4315.

(10) Ruggiero, E.; Richter, S. N. Viral G-Quadruplexes: New Frontiers in Virus Pathogenesis and Antiviral Therapy. *Annu. Rep. Med. Chem.* **2020**, *54*, 101−131.

(11) Zaccaria, F.; Paragi, G.; Fonseca Guerra, C. The Role of Alkali Metal Cations in the Stabilization of Guanine Quadruplexes: Why K+ Is the Best. *Phys. Chem. Chem. Phys.* **2016**, *18* (31), 20895−20904.

(12) Fonseca Guerra, C.; Zijlstra, H.; Paragi, G.; Bickelhaupt, F. M. Telomere Structure and Stability: Covalency in Hydrogen Bonds, Not Resonance Assistance, Causes Cooperativity in Guanine Quartets. *Chem. - Eur. J.* **2011**, *17* (45), 12612−12622.

(13) Brooks, T. A.; Kendrick, S.; Hurley, L. Making Sense of G-Quadruplex and i-Motif Functions in Oncogene Promoters. *FEBS J.* **2010**, *277*, 3459−3469.

(14) Zhao, C.; Song, H.; Scott, P.; Zhao, A.; Tateishi-Karimata, H.; Sugimoto, N.; Ren, J.; Qu, X. Mirror-Image Dependence: Targeting Enantiomeric G-Quadruplex DNA Using Triplex Metallohelices. *Angew. Chem.* **2018**, *130* (48), 15949−15953.

(15) Zhao, C.; Wu, L.; Ren, J.; Xu, Y.; Qu, X. Targeting Human Telomeric Higher-Order DNA: Dimeric G-Quadruplex Units Serve as Preferred Binding Site. *J. Am. Chem. Soc.* **2013**, *135* (50), 18786−18789.

(16) Neidle, S. Human Telomeric G-Quadruplex: The Current Status of Telomeric G-Quadruplexes as Therapeutic Targets in Human Cancer: G-Quadruplexes as Cancer Drug Targets. *FEBS J.* **2010**, *277* (5), 1118−1125.

(17) Abiri, A.; Lavigne, M.; Rezaei, M.; Nikzad, S.; Peyman, Z.; Mergny, J.-L.; Rahimi, H.-R. Unlocking G-Quadruplexes as Antiviral Targets. *Pharmacol. Rev.* **2021**, *73*, 897−923.
(18) Hognon, C.; Miclot, T.; Garcia-Iriepa, C.; Francés-Monerris, A.; Grandemange, S.; Terenzi, A.; Marazzi, M.; Barone, G.; Monari, A. Role of RNA Guanine Quadruplexes in Favoring the Dimerization of SARS Unique Domain in Coronaviruses. *J. Phys. Chem. Lett.* **2020**, *11* (14), 5661−5667.
(19) Tan, J.; Kusov, Y.; Mutschall, D.; Tech, S.; Nagarajan, K.; Hilgenfeld, R.; Schmidt, C. L. The "SARS-Unique Domain" (SUD) of SARS Coronavirus Is an Oligo(G)-Binding Protein. *Biochem. Biophys. Res. Commun.* **2007**, *364* (4), 877−882.
(20) Kusov, Y.; Tan, J.; Alvarez, E.; Enjuanes, L.; Hilgenfeld, R. A G-Quadruplex-Binding Macrodomain within the "SARS-Unique Domain" Is Essential for the Activity of the SARS-Coronavirus Replication−Transcription Complex. *Virology* **2015**, *484*, 313−322.
(21) Ruggiero, E.; Richter, S. N. Survey and Summary G-Quadruplexes and G-Quadruplex Ligands: Targets and Tools in Antiviral Therapy. *Nucleic Acids Res.* **2018**, *46*, 3270−3283.
(22) Yuan, Q.; Wu, Y.; Wang, J.; Lu, D.; Zhao, Z.; Liu, T.; Zhang, X.; Tan, W. Targeted Bioimaging and Photodynamic Therapy Nanoplatform Using an Aptamer-Guided G-Quadruplex DNA Carrier and Near-Infrared Light. *Angew. Chem., Int. Ed.* **2013**, *52* (52), 13965−13969.
(23) Zhao, C.; Qin, G.; Niu, J.; Wang, Z.; Wang, C.; Ren, J.; Qu, X. Targeting RNA G-Quadruplex in SARS-CoV-2: A Promising Therapeutic Target for COVID-19? *Angew. Chem., Int. Ed.* **2021**, *60* (1), 432−438.
(24) De Nicola, B.; Lech, C. J.; Heddi, B.; Regmi, S.; Frasson, I.; Perrone, R.; Richter, S. N.; Phan, A. T. Structure and Possible Function of a G-Quadruplex in the Long Terminal Repeat of the Proviral HIV-1 Genome. *Nucleic Acids Res.* **2016**, *44* (13), 6442−6451.
(25) Marquevielle, J.; Kumar, M. V. V.; Mergny, J. L.; Salgado, G. F. 1H, 13C, and 15N Chemical Shift Assignments of a G-Quadruplex Forming Sequence within the KRAS Proto-Oncogene Promoter Region. *Biomol. NMR Assignments* **2018**, *12* (1), 123−127.
(26) Kerkour, A.; Marquevielle, J.; Ivashchenko, S.; Yatsunyk, L. A.; Mergny, J. L.; Salgado, G. F. High-Resolution Three-Dimensional NMR Structure of the KRAS Proto-Oncogene Promoter Reveals Key Features of a G-Quadruplex Involved in Transcriptional Regulation. *J. Biol. Chem.* **2017**, *292* (19), 8082−8091.
(27) Mark, P.; Nilsson, L. Structure and Dynamics of the TIP3P, SPC, and SPC/E Water Models at 298 K. *J. Phys. Chem. A* **2001**, *105* (43), 9954−9960.
(28) Perez, A.; Marchán, I.; Svozil, D.; Sponer, J.; Cheatham, T. E.; Laughton, C. A.; Orozco, M. Refinement of the AMBER Force Field for Nucleic Acids: Improving the Description of Alpha/Gamma Conformers. *Biophys. J.* **2007**, *92* (11), 3817−3829.
(29) Zgarbová, M.; Otyepka, M.; Šponer, J.; Mládek, A.; Banáš, P.; Cheatham, T. E.; Jurečka, P. Refinement of the Cornell et Al. Nucleic Acids Force Field Based on Reference Quantum Chemical Calculations of Glycosidic Torsion Profiles. *J. Chem. Theory Comput.* **2011**, *7* (9), 2886−2902.
(30) Lindorff-Larsen, K.; Piana, S.; Palmo, K.; Maragakis, P.; Klepeis, J. L.; Dror, R. O.; Shaw, D. E. Improved Side-Chain Torsion Potentials for the Amber Ff99SB Protein Force Field. *Proteins: Struct., Funct., Genet.* **2010**, *78* (8), 1950.
(31) Phillips, J. C.; Braun, R.; Wang, W.; Gumbart, J.; Tajkhorshid, E.; Villa, E.; Chipot, C.; Skeel, R. D.; Kalé, L.; Schulten, K. Scalable Molecular Dynamics with NAMD. *J. Comput. Chem.* **2005**, *26* (16), 1781−1802.
(32) Gattuso, H.; Spinello, A.; Terenzi, A.; Assfeld, X.; Barone, G.; Monari, A. Circular Dichroism of DNA G-Quadruplexes: Combining Modeling and Spectroscopy to Unravel Complex Structures. *J. Phys. Chem. B* **2016**, *120* (12), 3113−3121.
(33) Terenzi, A.; Gattuso, H.; Spinello, A.; Keppler, B. K.; Chipot, C.; Dehez, F.; Barone, G.; Monari, A. Targeting G-Quadruplexes with Organic Dyes: Chelerythrine−DNA Binding Elucidated by Combining Molecular Modeling and Optical Spectroscopy. *Antioxidants* **2019**, *8* (10), 472.
(34) Gattuso, H.; Garcia-Iriepa, C.; Sampedro, D.; Monari, A.; Marazzi, M. Simulating the Electronic Circular Dichroism Spectra of Photoreversible Peptide Conformations. *J. Chem. Theory Comput.* **2017**, *13* (7), 3290−3296.
(35) Neidle, S. Quadruplex Nucleic Acids as Targets for Anticancer Therapeutics. *Nature Reviews Chemistry* **2017**, *1*, 0041.
(36) Tian, T.; Chen, Y. Q.; Wang, S. R.; Zhou, X. G-Quadruplex: A Regulator of Gene Expression and Its Chemical Targeting. *Chem.* **2018**, *4* (6), 1314−1344.

https://doi.org/10.1021/acs.jpclett.1c03071
J. Phys. Chem. Lett. 2021, 12, 10277−10283